JOURNAL OF MATERIALS SCIENCE 23 (1988) 4392–4398

Structure of amorphous boron

MASAYOSHI KOBAYASHI
The Institute of Physical and Chemical Research Wako, Saitama, 351-01 Japan

The short range order structure of amorphous boron is studied. Three sample materials of different appearances, film, whisker and fibre, are prepared by chemical vapour deposition by the reduction of BCl_3 with hydrogen. The reduced radial distribution functions (reduced RDFs) derived from their X-ray or electron diffraction patterns are found to be almost identical among the three samples. The reduced RDFs are compared with those calculated for the four crystalline modifications of boron, i.e. α-rhombohedral, α-tetragonal, β-tetragonal and β-rhombohedral boron. The reduced RDFs of amorphous boron are found to be similar to those of the β-tetragonal and β-rhombohedral boron. From the similarity of physical and chemical properties and co-existence in deposition, the short range order structure of amorphous boron is shown to be closer to that of the β-rhombohedral modification.

1. Introduction

Four crystalline modifications of boron are known to exist, α-rhombohedral boron [1], β-rhombohedral boron [2], α-tetragonal boron [3] and β-tetragonal boron [4]. Besides these modifications there exists amorphous boron which has been prepared by physical vapour deposition (PVD) [5, 6] or chemical vapour deposition (CVD) [7–10], pyrolysis [11, 12], or rapid cooling [13]. These amorphous borons give characteristic X-ray or electron diffraction patterns of diffuse haloes having nearly equal d spacings.

Although the short range order (SRO) structure of polycrystalline boron was derived by Godfray and Warren [14] through a radial distribution function (RDF) method [15] from its X-ray diffraction pattern, the SRO structure of amorphous boron was first reported by Katada [5] from its electron diffraction pattern. He proposed the existence and random arrangement of the B_{12} icosahedron which is the substructural unit common to all crystalline modifications of boron. Badzian [8] subsequently obtained the radial distribution function (RDF) of the amorphous boron film prepared by CVD from its X-ray diffraction pattern. He also deduced the icosahedral arrangement of boron and proposed that the structure of amorphous boron was a frozen stage in the transition from α-rhombohedal into β-rhombohedral boron. On the other hand different propositions were made for the SRO structure of amorphous boron obtained by PVD from both electron [16] and X-ray diffraction [6] that the arrangement of the B_{12} icosahedron was close to that of α-tetragonal boron. There is no consensus on the SRO structure of amorphous boron despite the use of similar RDF methods, except on the existence of the B_{12} icosahedron. The question is still open to discussion.

In the present work three kinds of amorphous boron samples with different appearances, film, whisker, and fibre, were prepared by CVD. The reduced RDFs were derived from their X-ray or electron diffraction patterns. The derived reduced RDFs for amorphous boron were compared with those calculated from the structural data of the four crystalline modifications of boron and found to be similar to those of β-tetragonal and β-rhombohedral boron. By comparing the physical and chemical properties of the amorphous boron and the β-rhombohedral modification, the arrangement of the B_{12} icosahedron in the amorphous boron was concluded to be closer to that of the β-rhombohedral modification.

2. Experimental procedure

2.1. Sample preparation

The CVD method with a gas flow system was used. The BCl_3 sample (99.99%) purchased from Matheson was purified through four-step fractional distillation. Hydrogen used was of high purity grade H_2 (99.99%) and was further purified through a palladium-alloyed film eliminating impurities up to 0.1 p.p.m. The hydrogen gas was first led (flow rate 0.5 to 1 litre min^{-1}) to a cold trap in which BCl_3 was kept. The partial pressure of BCl_3 in the mixed gas was controlled by the temperature of the cold trap (-47 to 0° C). The total pressure of the mixed gas was slightly over 1 atm. The mixed gas was led to reaction vessels of different types for CVD as follows.

The amorphous boron film (Sample A) was deposited on a transparent silica glass tube (o.d. 10 mm. length ~ 300 mm) in which an electric heater was inserted. The deposition temperature of 800 to 850° C was measured by an optical pyrometer. Fig. 1 shows a scanning electron microscope (SEM) pattern of $\sim 2\,\mu$m thick as-grown film with a grey metallic lustre. Its density was 2.33 g cm^{-3} (as-deposited film) and 2.39 g cm^{-3} (crushed down into powder) which were measured by a density-gradient tube method. Hence the film has $\sim 2.5\%$ porosity. Qualitative analyses by X-ray microanalyser (XMA) and emission

0022–2461/88 $03.00 + .12

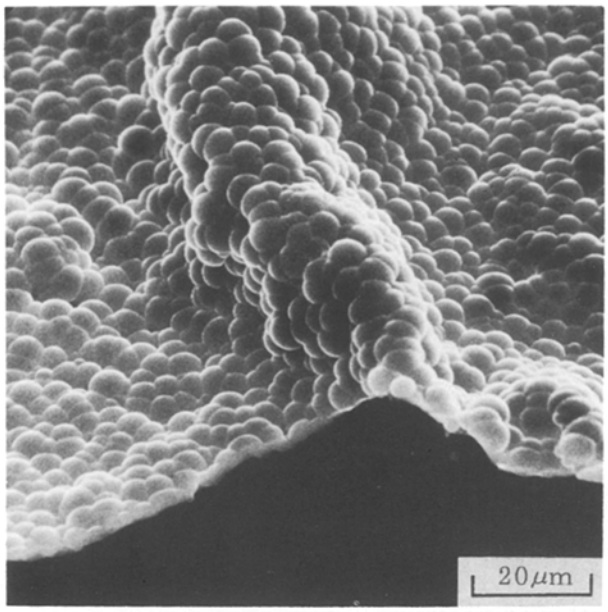

Figure 1 SEM pattern of ~2 μm thick as-grown boron film with grey metallic lustre detached from the silica glass tube (Sample A). The deposition temperature ranged from 800 to 850° C, the BCl_3 cold trap temperature was ~31° C and the H_2 flow rate 0.5 l min^{-1}.

spectroscopy did not show any other appreciable amount of elements besides boron and silicon. Quantitative wet chemical analysis showed the silicon content to be 0.13 wt %.

The whisker-like sample (Sample B) was deposited inside small silica glass tubes (o.d. 10 mm, length 100 mm). To increase the area of deposition four silica glass tubes were placed at the centre of a transparent silica glass reaction tube (o.d. 30 mm, i.d. 26 mm, length 640 mm) which was heated by a horizontal clamshell-type electric furnace. The temperature of the deposition zone was measured to be 770 to 830° C by a thermocouple. The sample was grown gregariously among clusters of boron globules with a black metallic lustre. Microphotographs of the sample are shown in Fig. 2 where Fig. 2a shows the clusters of boron globules and Fig. 2b the thread or whisker-like deposits. Besides these globules, small pieces of thin metallic-lustre films like Sample A were co-deposited.

TABLE I Deposition conditions for Samples A, B, and C

Sample	Substrate	Temperature (° C)		H_2 flow rate (l min^{-1})
		Deposition	Trap	
A (film)	Fused SiO_2	800 to 850	−31	0.5
B (whisker)	Fused SiO_2	770 to 830	−47	1.0
C (fibre)	Copper	~800	0	0.5

The fibre-like deposit (Sample C) was obtained at ~800° C on a deoxygenated copper tube (o.d. 12 mm, length 40 mm). The tube was heated by inserting tightly the silica glass tube used for preparation of Sample A. The growth products were black, velvety and uniform in their appearance. An SEM pattern of the fibre-like products covering the surface with 20 to 40 μm thickness is shown in Fig. 3. The products have many branches in contrast to the straight whiskers in Sample B.

The deposition conditions used for the three samples are listed in Table I.

2.2. X-ray and electron diffraction

Powdered Sample A was placed in a thin-walled glass capillary tube (o.d. ~0.5 mm) for a Debye–Scherrer powder camera with 114.6 mm diameter. Copper $K\alpha$ radiation filtered with nickel foil was used with a typical exposure time of about 8 h. The X-ray diffraction pattern consisted of four diffuse haloes. Similar patterns were obtained when as-grown thin films of Sample A were used. However, clusters of black globules and chains of small spheres, which were co-deposited with Sample B, showed X-ray diffraction powder patterns analogous to the β-rhombohedral boron type, with haloes for the former and without haloes for the latter.

An electron microscope operated under an accelerating voltage of 50 kV was used for a transmission electron diffraction (TED) measurement with the camera length of about 60 cm. Samples B and C were fixed directly on copper-sheet meshes. The electron microphotograph of Sample B and its TED pattern are shown in Fig. 4, and those of Sample C are also displayed in Fig. 5. In the TED patterns of both

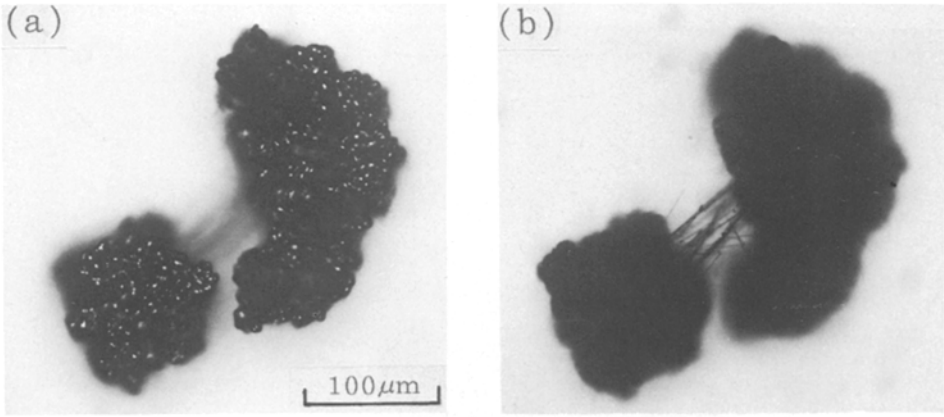

Figure 2 Microphotographs of clusters of boron globules with black metallic lustre. (a) Filamentary deposits are to be observed but out of focus; (b) thread- or whisker-like deposits are seen in focus (Sample B). The deposition temperature ranged from 770 to 830° C, the BCl_3 cold trap temperature was ~47° C and the H_2 flow rate 1.0 l min^{-1}.

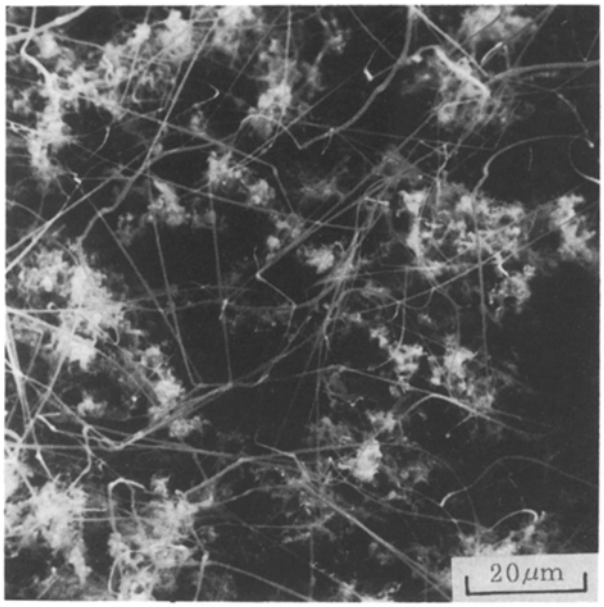

Figure 3 SEM pattern of fibre-like deposits as grown on copper tube substrate (Sample C). The deposited growth products are black and velvety, covering the surface with 20 to 40 μm thickness with many branches. The deposition temperature was ~ 800° C, the BCl_3 cold trap temperature 0° C and the H_2 flow rate 0.51 min^{-1}.

Samples B and C, four diffuse haloes are observed as in Sample A. In Table II, d spacings of these haloes are presented with the equivalents of various amorphous boron samples which have been reported in the literature [6–13].

3. Collection and reduction of diffraction intensities

The collection and reduction of the X-ray and electron diffraction intensities were performed as described elsewhere [17–21], with the exception that a polarization correction was applied to the X-ray scattering intensities as usual, but an absorption correction was ignored for such a light element as boron. The essence of the method will, however, be recapitulated to facilitate the discussion. The following numerical expressions are simplified for monatomic clusters.

The interference intensity function, $i(s)$, and the reduced RDF(observed), $G(r)_{obs}$, are expressed as

$$i'(s) = \frac{I'(s)_{obs} - I'(s)_{back}}{f_e^2(s)} \exp(-As^2) \quad (1)$$

and

$$G(r)'_{obs} = 4\pi rz[g'(r) - g'_0] = \frac{2}{\pi}\int_0^{s_{max}} si'(s) \sin(rs)ds \quad (2)$$

The primed terms mean their arbitrariness with respect to units. The intensities $I'(s)_{obs}$ and $I'(s)_{back}$ are the observed X-ray or electron scattering intensity and the structure-independent scattering intensity or background, respectively. The elementary scattering factor per single electron or nuclear charge is given by $f_e(s) = f(s)/z$ for a monatomic specimen where $f(s)$ and z are the atomic scattering amplitude for the incident X-ray or electron and the atomic number, respectively. An artificial temperature factor $\exp(-As^2)$ is introduced to minimize termination-of-series errors at the experimental upper limit s_{max}. The value of A in the exponential term was determined so that the factor become 0.1 at s_{max}. The scattering function is defined by $s = 4\pi \sin\theta/\lambda$ in which 2θ is the scattering angle and λ is the X-ray or electron wavelength. The electron or nuclear charge density function and its average are presented by $g'(r)$ and g'_0, and the latter is normalized to g_0 of the structure model.

The scattering intensities from monatomic atoms composing a non-crystalline cluster are derived through a partly modified Debye scattering intensity equation as

$$I''(s)_{calc} = \sum_i^N f^2(s) + f^2(s) \sum_i^{i\neq j} \sum_j^{i\neq j} \times \frac{\sin(sr_{ij})}{sr_{ij}} \exp(-Bs^2) \quad (3)$$

$$I(s)_{calc} = I''(s)_{calc}/N \quad (4)$$

where r_{ij} is the interatomic distance between atoms i and j, B is equivalent to a temperature factor, and N is the total number of atoms constituting the cluster in the microcrystalline model of boron concerned. The reduced RDF(calculated), $G(r)_{calc}$, is obtained from Equation 2 by substituting $I(s)_{calc}$ in Equation 4 and $f^2(s)$ of the atom into $I'(s)_{obs}$ and $I'(s)_{back}$ in Equation 1, respectively.

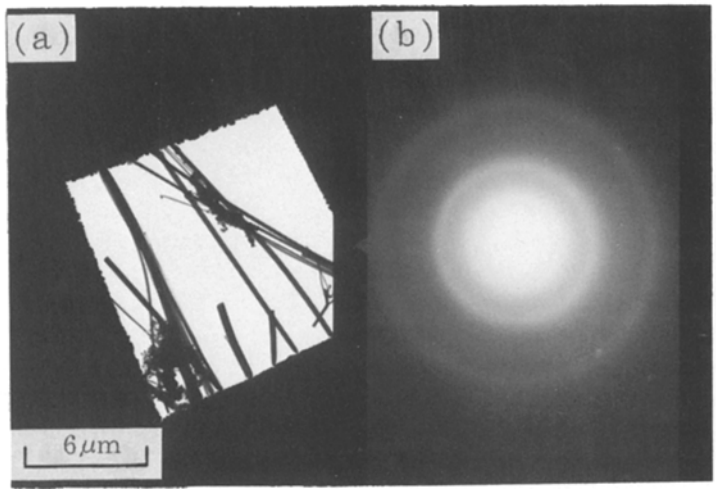

Figure 4 (a) Electron microphotograph of Sample B (whisker-like deposit) and (b) its TED pattern where four diffuse haloes are observed.

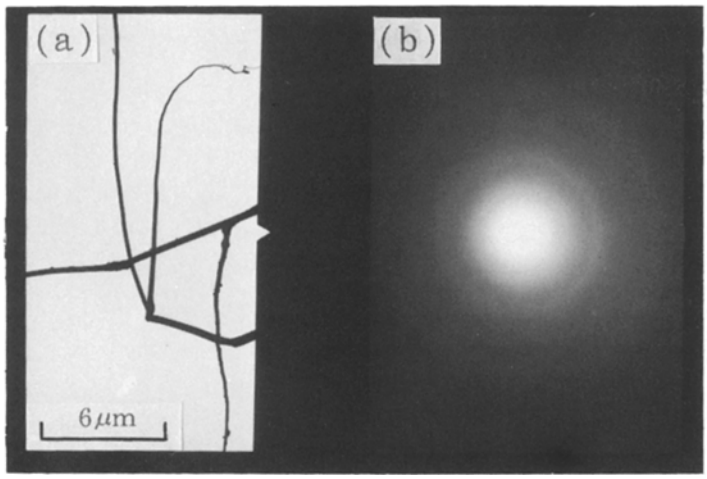

Figure 5 (a) Electron microphotograph of Sample C (fibre-like deposit) and (b) its TED pattern in which four diffuse haloes are observed.

4. Results and discussion

As shown in Table II, the d spacings of amorphous boron listed are almost equal regardless of the preparative methods. The filamentary appearance of amorphous boron in Samples B and C is a striking contrast to the filamentary boron crystals of α-rhombohedral boron grown at ~1000° C [22] and β-rhombohedral boron at 1200 to 1300° C [23]. The nodule-like deposits found on Sample A were also amorphous [24].

Fig. 6 shows the $G(r)_{obs}$ plots where AX, BE, and CE denote Samples A, B, and C derived from X-ray (for Sample A) and electron (for Samples B and C) diffraction patterns through the RDF method, respectively. The undulations of AX, BE, and CE are similar up to r = ~0.9 nm except for the nearly truncated broad peak of BE centred at r = 0.58 nm. A fair agreement between AX and CE is obtained despite the different sample preparations and diffraction methods. The undulations of these $G(r)_{obs}$ plots that reflect the SRO structures are in good agreement with those of the RDF of Badzian [8] up to r = ~0.8 nm and of Palatnik *et al.* [6] up to r = ~0.6 nm from their X-ray diffraction patterns. This suggests that these amorphous borons have nearly the same SRO structures regardless of the preparative method.

The SRO structure thus obtained is, however, a statistical one and does not give any absolute structure. Then, it is necessary to compare the $G(r)_{obs}$ with the equivalent of a suitably selected structure model. Hence all the crystalline modifications of boron are used as the structure models. Although α-tetragonal boron is said not to be found without the presence of foreign atoms such as carbon or nitrogen [25–27], this modification is included, since these atoms are replaceable with boron, and their presence does not seem to affect appreciably the SRO structure of this modification. The $G(r)_{calc}$ plots calculated from the structural data of all the crystalline modifications are shown in Fig. 7 where AR, AT, BT, and BR stand for α-rhombohedral, α-tetragonal, β-tetragonal and β-rhombohedral boron, respectively. The first two coordination sphere peaks at r = ~0.18 and ~0.31 nm agree well among all four structure models. This is ascribed to the B_{12} icosahedron which is the

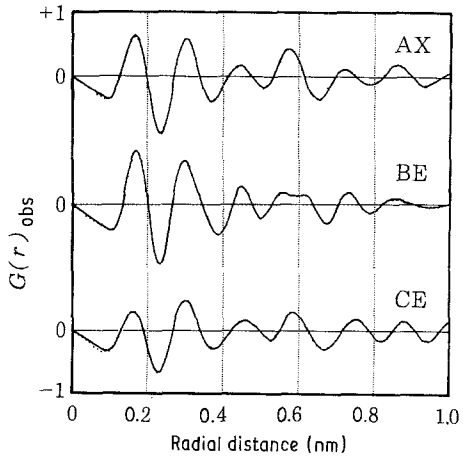

Figure 6 Observed $G(r)_{obs}$ plots derived through the RDF method from X-ray (for Sample A) and electron (for Samples B and C) diffraction patterns. AX, BE, and CE denote Samples A, B, and C, respectively. The ordinate is in units ($\times 10^4$) of $e^2 nm^{-2}$ or $+ne^2 nm^{-2}$ for X-ray or electron diffraction and the abscissa is the radial distance from an arbitrarily-selected central atom.

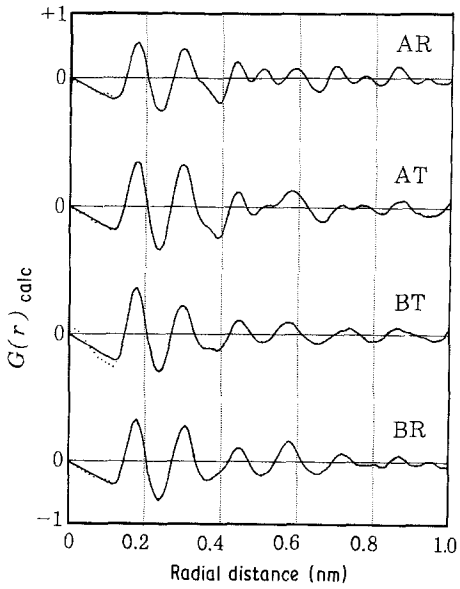

Figure 7 Comparison of calculated $G(r)_{calc}$ plots from structural data of four crystalline boron models. AR, AT, BT, and BR denote α-rhombohedral, α-tetragonal, β-tetragonal and β-rhombohedral boron, respectively. The ordinate is in units of 10^4 ($+ne^2 nm^{-2}$).

TABLE II *d* spacings of various amorphous boron samples (nm)*

PVD		CVD									Pyrolysis		
Palatnik *et al.* [6]		Gillespie [7]	Badzian [8]	Lindquist *et al.* [10]		Galasso *et al.* [9, 13]		Present work			Otte and Lipsitt [12]		Amberger and Dietze [11]
X	E	X	X	X	E	E [9]	(E) [13]†	X(A)	E(B)	E(C)	X	E	X
0.435	0.45	0.44	0.43	0.408 to 0.476	0.443	0.44	(0.44)	0.426	0.438	0.430	0.44	0.42 to 0.45	0.42
0.25	0.25	0.25	0.255	0.238 to 0.268	0.255	0.25	(0.25)	0.253	0.253	0.253	0.25	0.25 to 0.261	0.25
					0.213								
0.167		0.17	0.170	0.168 to 0.180	0.175			0.170	0.173	0.178	0.175	0.170 to 0.176	0.17
0.138	0.14	0.14	0.144	0.130 to 0.145	0.142	0.14	(0.14)	0.139	0.141	0.141	0.14	0.138 to 0.145	0.14
												0.12	
				0.11								0.11	
			0.094 to 0.084	0.094	0.0943							0.091	

*X and E mean X-ray and electron diffraction, respectively.
†Rapid cooling.

common structural unit for all these crystalline modifications of boron [5, 6, 8, 16]. The first nearest neighbour intra- and inter-icosahedral mean interatomic distance of ~ 0.18 nm corresponds to the first coordination sphere peak, and the second to the first third nearest neighbour intraicosahedral interatomic distances of ~ 0.28 and ~ 0.34 nm form an unresolved peak at $r = \sim 0.31$ nm, which agrees well with the observed second coordination sphere peak.

There remain, however, differences among the $G(r)_{calc}$ plots of crystalline models beyond the third coordination sphere peak at $r = \sim 0.45$ nm. In particular the small peak observed at $r = \sim 0.51$ nm in AR, the fourth coordination sphere peak, corresponds to the specific interatomic distance between adjacent icosahedra. In α-rhombohedral boron [1] the B_{12} icosahedron locates at the lattice point of the rhombohedral unit cell with the same orientation (in phase). So the B–B specific interatomic distances along the rhombohedral a axis and the a axis of the pseudo-hexagonal cell are ~ 0.506 nm for the former and ~ 0.491 nm for the latter. From convolution of these values the distance of ~ 0.50 nm is obtained. This value corresponds to the fourth coordination sphere peak at $r = \sim 0.51$ nm described above.

In AT the peak at $r = \sim 0.51$ nm is not so large as in AR. In α-tetragonal boron [3] there exist two types of intericosahedral linkage. One is lying along the pseudo-fivefold axis in parallel with the c axis of the cell (in phase) and the other is on the curved pseudo-fivefold axis (out of phase). In the former the specific interatomic distance of ~ 0.507 nm corresponds to the lattice constant $c = \sim 0.507$ nm. On this account, the peak at $r = \sim 0.51$ nm becomes small compared to that of AR, but the third and the fifth coordination sphere peaks at $r = \sim 0.44$ and ~ 0.58 nm become larger in the opposite way.

In BT and BR, no corresponding peak at $r = \sim 0.51$ nm is seen. This may be explained as follows. In the intericosahedral linkages in β-tetragonal boron [4] and the β-rhombohedral modification [2], the B_{12} icosahedra are linked along their pseudo-fivefold axes with a rotation of $\sim \pi/5$ with respect to each other (out of phase). The peak at $r = \sim 0.51$ nm is then hardly observed; instead the coordination sphere peaks at $r = \sim 0.44$ and ~ 0.58 nm become larger compared to those of AT. BT and BR show nearly the same undulations, indicating the similarity of their SRO structures, which is in agreement with the correspondence between the three-dimensional boron frameworks of β-rhombohedral and β-tetragonal boron [28, 29]. By comparing the $G(r)_{obs}$ plots in Fig. 6 with the $G(r)_{calc}$ plots of crystalline models in Fig. 7, it is found that the $G(r)_{obs}$ plots are more similar to the $G(r)_{calc}$ plots of BT and BR up to $r = \sim 0.85$ nm than to the equivalents of AR and AT. The former two are known as metastable and stable phases, respectively, of boron at high temperature, and the latter two are known as metastable at low temperature. This result is quite different from the previous ones obtained by the RDF method as described in Section 1. The fair agreement of $G(r)_{obs}$ to those of BT and BR beyond the second coordination sphere peak is noteworthy. This is quite a contrast to the general understanding that the similarity between the short-range order in amorphous and crystalline semiconductors mostly goes not much further than the second coordination sphere peak [30, 31]. In the present case of amorphous boron, the situation is quite different. The observed similarity is not simply due to a random arrangement of such a large substructure as the B_{12} icosahedron.

As described above the SRO structure of the amorphous boron is similar to those of β-tetragonal and β-rhombohedral boron. This suggests that the same kind of substructural framework of boron as in both β-tetragonal and β-rhombohedral modifications exists in the amorphous boron. This is explained as follows. After the structure elucidation of α-AlB_{12} [32], the structure of γ-AlB_{12} was determined [28]. The structure is based on a framework of boron icosahedra, that is, the bi-layered sheet of icosahedra forming a kagomé layer of interconnected B_{48}-(Td) units, a tetrahedron of four B_{12} icosahedra, or B_{144}-(Td) units which is the basic layer structure in the frameworks of γ-AlB_{12}, α-AlB_{12} and β-rhombohedral boron. Here the symbol inside the parentheses is in the standard Schoenflies notation [5]. It was subsequently found that the structure of β-tetrahedral boron [4] consists of a three-dimensional boron framework which is basically the same as that of α-AlB_{12}. The structural difference between β-tetragonal boron and the β-rhombohedral modification is only explained by postulating that in the large holes inside the B_{144}-(Td) unit B_{21} (C_2) [4] or B_{22} (C_2) [29] completed twinned icosahedra located in the former, and that B_{28}-(C_{3u}) triply condensed icosahedra do so in the latter [28].

Accordingly it is difficult to seek for further analogy to either β-tetragonal or β-rhombohedral boron based only on the observed $G(r)_{obs}$ of amorphous boron. However, the following chemical and physical properties are to be considered:

(i) β-rhombohedral boron is stable up to its melting point and crystallizes easily from its melt. By rapid cooling of the melt almost entirely amorphous boron is obtained except for a very little β-rhombohedral boron [13]. The amorphous boron thus obtained has nearly the same d-spacings as the other sources of amorphous boron prepared by CVD and PVD.

(ii) β-rhombohedral boron is co-deposited with amorphous boron by CVD at low temperature around 850° C [33], while the deposition temperature of β-tetragonal boron is confined to very narrow temperature ranges of 1150 to 1200° C [34] and 1220 to 1280° C [33].

The observed density $D_m = 2.39\,g\,cm^{-3}$ of Sample A is slightly larger than the published values of 2.30 [8], 2.35 [11] and 2.37 [10], although the calculated X-ray density D_x of β-rhombohedral boron crystal is 2.29 and the measured value, D_m, is $2.35\,g\,cm^{-3}$ [2]. In respect to this, some speculations can be made. The most stable β-rhombohedral boron has the smallest value of the coefficient of space-filling among all the crystalline modifications of boron [35] and is characterized by an exceptionally loose filling of the structure. Furthermore, some of the established atomic

coordinates of this modification are not fully occupied [2]. This also affords 18 vacant substitutional sites per hexagonal unit cell. So there are many more opportunities for additional boron atoms to enter into the cell interstitially or substitutionally, especially in the case of amorphous boron. The presently observed D_m value of $2.39\,g\,cm^{-3}$ corresponds to the hexagonal unit-cell boron content of B_{329}, which exceeds the theoretical unit-cell content of B_{315} by 14. However, if the β-rhombohedral boron modification is supposed as the SRO structure of the amorphous boron, the wide ranges of variation of D_m values in amorphous boron will be easily understood.

5. Conclusions

These various lines of evidence may lead to the conclusion that the SRO structure of the amorphous boron is more similar to that of β-rhombohedral boron than to that of the β-tetragonal modification.

Acknowledgements

The author wishes to thank Dr I. Higashi for his encouragement, and for helpful discussions and suggestions on this work. Thanks are also due to Dr M. Uda and Dr Y. Takahashi for performing the electron diffraction and chemical analyses. The author would further like to express his appreciation to Dr M. Takami for his stimulation and a critical reading of the manuscript.

References

1. B. F. DECKER and J. S. KASPER, *Acta Crystallogr.* **12** (1959) 503.
2. J. L. HOARD, D. B. SULLENGER, C. H. L. KENNARD and R. E. HUGHES, *J. Solid State Chem.* **1** (1970) 268.
3. J. L. HOARD, R. E. HUGHES and D. E. SANDS, *J. Amer. Chem. Soc.* **80** (1958) 4507.
4. M. VLASSE, R. NASLAIN, J. S. KASPER and K. PLOOG, *J. Solid State Chem.* **28** (1979) 289.
5. K. KATADA, *Jpn J. Appl. Phys.* **5** (1966) 582.
6. L. S. PALATNIK, A. A. KOZ'MA and A. A. NECHITAILO, *Sov. Phys. Crystallogr.* **28** (1983) 73.
7. J. S. GILLESPIE Jr., *J. Amer. Chem. Soc.* **88** (1966) 2423.
8. A. R. BADZIAN, *Mater. Res. Bull.* **2** (1967) 987.
9. F. GALASSO, D. KUEHL and W. TICE, *J. Appl. Phys.* **38** (1967) 414.
10. P. F. LINDQUIST, M. L. HAMMOND and R. H. BRAGG, *ibid.* **39** (1968) 5152.
11. E. AMBERGER and W. DIETZE, *Z. anorg. allg. Chem.* **332** (1964) 131.
12. H. M. OTTE and H. A. LIPSITT, *Phys. Status Solidi* **13** (1966) 439.
13. F. GALASSO, R. VASLET and J. PINTO, *Appl. Phys. Lett.* **8** (1966) 331.
14. T. N. GODFREY and B. E. WARREN, *J. Chem. Phys.* **18** (1950) 1121.
15. B. E. WARREN, H. KRUTTER and O. MORNINGSTAR, *J. Amer. Ceram. Soc.* **19** (1936) 202.
16. Y. G. POLTAVTSEV, V. P. ZAKKAROV and V. M. POZDNYAKOVA, *Sov. Phys. Crystallogr.* **18** (1973) 270.
17. I. L. KARLE and J. KARLE, *J. Chem. Phys.* **17** (1949) 1052.
18. J. KARLE and I. L. KARLE, *ibid.* **18** (1950) 957.
19. M. KOBAYASHI and M. UDA, *J. Non-Cryst. Solids* **41** (1980) 241.
20. M. KOBAYASHI, in "Passivity of Metals and Semiconductors, Proceedings of 5th International Symposium on Passivity, Bombannes, France, May/June 1983, edited by M. Froment (Elsevier, Amsterdam, 1983) p. 169.
21. M. KOBAYASHI, M. UDA and S. SUZUKI, *Boshoku Gijutsu (Corrosion Eng.* **33** (1984) 694.
22. J. P. SITARIK and W. C. ELLIS, *J. Appl. Phys.* **37** (1966) 2399.
23. I. AHMAD and W. J. HEFFERNAN, *J. Electrochem. Soc.* **118** (1971) 1670.
24. G. E. VUILLARD, A. LUGUE and L. VANDENBULCKE, *J. Less-Common Metals* **47** (1976) 235.
25. E. AMBERGER and K. PLOOG, *ibid.* **23** (1971) 21.
26. K. PLOOG, H. SCHMIDT, E. AMBERGER and G. WILL, *ibid.* **29** (1972) 161.
27. G. WILL and K. H. KOSSOBUTZKI, *ibid.* **43** (1976) 33.
28. R. E. HUGHES, M. E. LEONOWICZ, J. T. LEMLEY and L. -T. TAI, *J. Amer. Chem. Soc.* **99** (1977) 5507.
29. I. HIGASHI, in "Boron-Rich Solids", Proceedings of International Conference on the Physics and Chemistry of Boron and Boron-Rich Borides (AIP Conference Proceedings 140), Albuquerque, New Mexico, July 1985, edited by D. Emin, T. Aselage, C. L. Beckel, I. A. Howard and C. Wood (American Institute of Physics, New York, 1986) p. 1–10.
30. R. GRIGOROVICI, *J. Non-Cryst. Solids* **1** (1969) 303.
31. M. V. COLEMAN and D. J. D. THOMAS, *Phys. Status Solidi* **24** (1967) Klll.
32. I. HIGASHI, T. SAKURAI and T. ATODA, *J. Solid State Chem.* **20** (1977) 67.
33. L. VANDENBULCKE and G. VUILLARD, *J. Less-Common Metals* **67** (1979) 65.
34. K. PLOOG, *ibid.* **31** (1973) 15.
35. D. V. KHANTADZE and N. J. TOPURIDZE, *ibid.* **117** (1986) 105.

Received 3 November 1987
and accepted 23 February 1988